A 3D Simulation-based Approach to Analyze Heavy Ions-induced SET on Digital Circuits

A 3D Simulation-based Approach to Analyze Heavy Ions-induced SET on Digital Circuits

L. Sterpone, *Member, IEEE*, F. Luoni, S. Azimi., *Member, IEEE* and B. Du, *Member, IEEE*

***Abstract*—Radiation-induced Single Event Transients (SETs) are the leading cause of mal-operations in CMOS nanometric integrated circuits. The increasing complexity of advanced CMOS digital circuits makes SET effects investigation a rising challenge. In this work, we propose a three-dimension oriented simulation approach able to model the passage of heavy ions particles through the physical structures of modern digital circuits implemented with ultra-nanometric manufacturing processes. The proposed approach is able to generate the transient voltage pulse in response to a heavy ion track and identify the effects of the sensitive volume and contact structure. We present heavy ion radiation test experiments performed on a 65 nm Flash-based CMOS technology process and, as proof-of-concept, we successfully compared the SET cross-sections showing comparable results.**

***Keywords*—Single Event Transient, Heavy Ions, Simulation, Layout, Radiation Effects, 3D**

I. INTRODUCTION

THE impact of radiation-induced Single Event Transients (SETs) on Integrated Circuits (ICs) adopted in harsh environments is drastically increasing. As widely demonstrated, due to the increase of transistor density for the new CMOS technology, the probability of a single heavy ion to provoke an SET in a circuit or more nodes is increasing [1]. In particular, for ultra-nanometer (e.g., below 100 nm) technology nodes, the charge collection basic mechanisms on multiple nodes become the most relevant phenomena [2] since the elementary logic gates of the integrated circuits are a composition of various metallization layers, junctions and insulators organized and interposed within a unique nano-metric volume [3]. The usage of new materials for the electronic part is another important aspect to be considered. These materials do not have a well-documented particle-matter interaction and may provide different charge sharing and collection mechanisms [4]. Thus, the impact of increased transistor density, use of new materials and overall design complexity have made traditional statistically-oriented techniques obsolete [5].

In the last decades, studies have investigated how the digital circuit layout geometries can influence the SET measurement analysis. Typically, most of the studies considered inverter structures since they are more easily analyzed by heavy ion radiation experiments [6]. In order to achieve statistically relevant results, prior research analyzed chains with more than 1,000 inverters [7] showing how SETs can have different shape during the propagation through various combinational gates [8]. We performed the same type of analysis on Flash-based Field Programmable Gate Arrays (FPGAs) adopting 130 nm VersaTile cells [9] and demonstrated that the propagation phenomena is not only related to the source SET but also on the topology and types of logic cells [10]. Considering research works more focused on the internal structure of the cell, extremely relevant results have been published by Amusan et al. in [11]. Recently, it has been demonstrated that the SET pulse width is directly dependent on the transistor drive current and cross-section for FinFET technology [12]. These studies are relevant because they allow isolating the physical basic mechanisms behind the SET pulse generation. However, they are not suitable to support an efficient analysis of the SET performance of an entire IC [13]. In fact, for advanced ICs the problem involves the multiplicity of the logic cells in conjunction with the effects of the metallization within and between the cells [14].

In order to tackle this problem and provide a global approach that includes physical mechanism to model the SET generation and sequential modeling to describe the propagation of the SET pulses across the circuit, two different types of SET predictive methods were found in the literature.

The first one is the MUSCA-SEP3 tool [15] which is applicable to ASIC circuits. This tool is based on a sequential modeling that starts with the device and material environment and also includes the radiation response of the "struck" device generating electron/hole pairs. It simulates the transportation and collection mechanism and finally elaborates the circuit effects that allows the designer to statistically compute the expected Soft Error Rate (SER). The second one is the Single Event Transient Analysis (SETA) tool [16] that performs the Single Event Transient Analysis for FPGA-based circuits. This tool performs an exhaustive evaluation of SET overall circuit sensitive nodes mapped on the FPGA. Thanks to the Propagation Induced Pulse Broadening (PIPB) effect analysis, the SETA tool is able to provide an accurate prediction of the most critical circuit resources and to provide maximal pulse width information allowing selective SET filtering.

The main contribution of this paper is the realization of a new simulation approach, based on three-dimensional

The manuscript was submitted on 1st November 2019, Revised on 30 April 2020 and Accepted on 20 June 2020.

Luca Sterpone, Sarah Azimi and Boyang Du are with Dipartimento di Automatica e Informatica, Politecnico di Torino, Torino, Italy (e-mail: luca.sterpone@polito.it). F. Luoni is with the Helmholtzzentrum für Schwerionenforschung, GSI, Darmstadt, Germany.

simulation, able to model and simulate the effects of the passage of heavy ions into the silicon matter of modern Integrated Circuits and to generate the transient voltage pulse response on the output nodes. The main innovation of our methodology is the capability of modeling the heavy ion tracks through the different volumes of digital circuit cells. This has been possible thanks to development of a novel method for the ion track propagation through the cell, which is capable of considering the charge sharing effect when the ion traverses multiple cell layers. Furthermore, the developed tool, named Rad-Ray, is able to propagate the charge towards the cell output nodes and to extend the voltage glitch propagation to the whole circuit netlist enabling the possibility to calculate an effective SET cross-section of the circuit in relation to the type of heavy ion and LET used. We applied the Rad-Ray tool to a 65 nm model of a Look-Up Table (LUT) used in Flash-based FPGA and compared the results obtained by radiation test experiments executed at the UCL, Cyclotron of Louvain-la-Neuve. The results obtained provide a match between the SET cross-section per LUT calculated by Rad-Ray and the radiation test result.

The paper is organized as follows. Section II provides an overview of the related works in the field of 3D simulation of radiation effects and the Single Event Transient phenomena. Section III describes the background theory related to the basic mechanism of the heavy ion track propagation within Silicon matter. The developed three-dimensional simulation approach is presented in Section IV, while the experimental results including heavy ion radiation test campaigns, 3D simulation and the comparative analysis are reported in Section V. Finally, conclusions are drawn in Section VI.

II. Related Works

Simulation approaches have long been adopted to provide meaningful analysis of radiation effects on digital devices. In principle these methods were based on single dimensional drift diffusion modeling [17] and later focused on the transient radiation response as Single Event Upsets [18] by means of numerical modeling. A pioneering work was presented by P. E. Dodd in [19] where three-dimensional simulation of radiation effects in circuits model the physical mechanism of the charge deposition and transportation for CMOS structure adopting both two and three-dimensional computational methods. An evolution of the previous approaches has been proposed by Warren et al. thanks to the development of an energy deposition tool (MRED) [20] able to simulates radiation transport into integrated circuits [21] [22] [23]. However, this method does not include the complete topology and volumes organization of the VLSI cell under analysis, which is necessary to effectively analyze advanced integrated circuits.

As digital circuit geometrical structures continue to scale down to ultra-nanometric miniaturization, the probability that more than one transistor is affected by charge collection has become relevant, in particular for CMOS technology processes below 100 nm as demonstrated in [24]. As a consequence, it is fundamental to evaluate multiple-transistor effects by modeling the total collected charge with respect to the radiation strike location in order to better analyze and mitigate ultra-nanometric digital circuits. However, one of the main challenges of this goal, is the physical characteristics of the technology adopted for implementing each combinational and sequential cell.

In particular, the physical design libraries that are used to manufacture the silicon mask of digital circuits, generally include hundreds of standard cells to implement various functionality of a circuit. Besides, each one of them has a different layout and is composed of thousands of nanometric volumes that will generate a different impact on transient effects when a radiation particle strikes.

Given this scenario, two main concerns arise: firstly, cells can be placed and routed in an indefinite manner when mapped on the silicon; secondly, each cell is characterized by thousands of nanometric volumes that make the radiation effect evaluation much more complex.

Recently, two tools have been used to pursue the objective to analyze the complexity of modern digital circuits. The first tool that can be applied to an ASIC circuit design is MUSCA-SEP3 [15]. The main computational core of this tool is a sequential modeling that includes the physical device and environment characteristics and is able to compute the interaction of different radiation particles in the device, generate the electron/hole pairs due to the radiation strike, perform the transportation and collection mechanism and finally statistically elaborates the Soft Error Rate (SER). The second approach able to perform the propagation on structured digital circuits such as FPGA devices is the Single Event Transient Analysis (SETA) tool. In a manner different from the first analysis, this tool executes an exhaustive evaluation of the SET circuit sensitive nodes and implements the Propagation Induced Pulse Broadening (PIPB) effect analysis [8]. Thus, it is able to provide an accurate prediction of the most critical gate in the target circuit and to provide information about the pulse width.

III. Heavy Ion Track Basic Mechanisms

The heavy ion track basic mechanisms allow characterizing the ion track propagation based on the nature and energy of the ion radiation and the angle of incidence on the sensitive surface. In this section, we briefly describe the interaction models we implemented within the Rad-Ray tool.

The first interaction we implemented has been the ion interaction with the electrons of the surrounding medium by exciting or eventually ionizing its atoms. In this second case, we modeled secondary electrons with their energy after the collision. We considered the level of energy in eV. In cases where it is lower than the matter threshold (e.g., 100 eV for the SiO_2), the electrons release their energy in the material creating clusters of other ionized or excited atoms as illustrated in the example reported in Fig. 1. In cases where the electron energy is between 100 eV and 500 eV, it can generate high-energy delta rays. During the propagation of the delta rays, secondary blobs of energies with high energy can be generated too. Finally, in the case that the electron's energy

exceeds 500 eV, it can generate a high-energy delta ray in the form of secondary trajectories. The secondary trajectories have a very different shape than the original heavy ion one, since the ion mass is much bigger than that of the electrons it collides with, so it loses much less energy in the collision compared with the secondary electrons. Please note that we did not model Auger electrons and secondary photons due to the electronic relaxation generally characterizing the Si lattice.

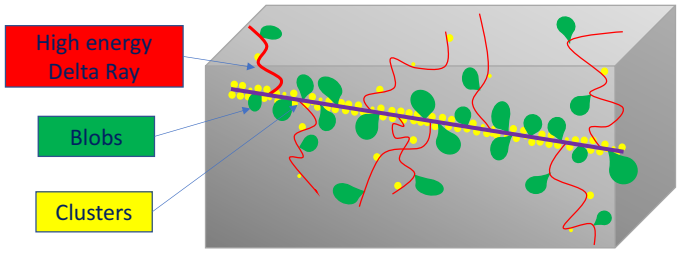

Fig. 1. An example of heavy ion track basic mechanisms modelled by the Rad-Ray tool during one ion propagation into a SiO_2 volume.

In order to model the generation of primary and secondary clusters, blobs and high-energy delta rays, we developed a probability density model that can be tuned with respect to the heavy-ion used during a simulation based on the results achieved by H. Xu and reported in [17].

Our developed model provides a probability density value for the generation of each ion-matter effect considered including primary clusters, primary blobs, secondary clusters and secondary blobs, where each blob represents an energy deposition cluster. The charge propagation effect is extended modeling the different volumes included in the Ion range longitudinal distribution. Furthermore, its effect is related to the bias condition of the cell that defines for each individual volume the kind of response with respect to the traversing ion. We report, in Fig. 2, the plot of the ion-matter event probability density of the Xe heavy ion at the LET of 62.5 MeV/mg/cm^2.

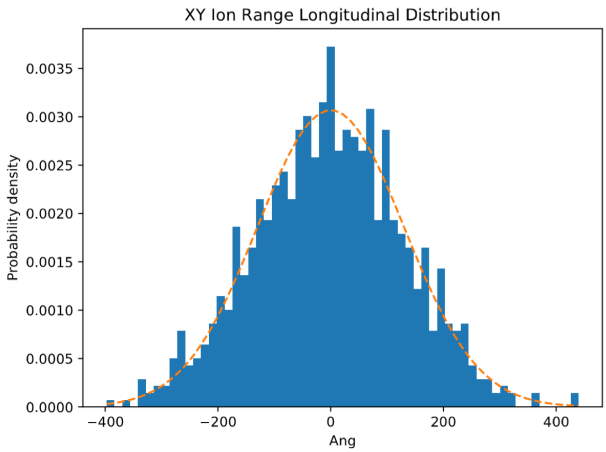

Fig. 2. The probability density plotted in the form of Ion Range Longitudinal distribution for the Xe heavy ion at the LET of 62.5 MeV/mg/cm^2.

IV. The Developed 3D Simulation Approach

The developed 3D simulation approach starts by loading the Graphic Data System-II (GDS-II) description of the circuit under analysis. The overall execution flow is shown in Fig. 3. The GDS file is the result of the circuit design and is the file transmitted to the foundries for the fabrication of the integrated circuit. The proposed 3D simulation approach uses three ancillary files:

1. *Layer material and depth*: A file that contains the type of material (e.g., metallization type, polysilicon gates or crystalline silicon bulk etc.) and the depth of each layer in ångström.
2. *Data Signal*: A file describing the voltage level status of each volume of the circuit under analysis.
3. *Heavy Ion Energy Loss*: A file containing the heavy ion energy loss released for each layer and type of material without considering any bias condition. An external tool such as TRIM can generate this file.

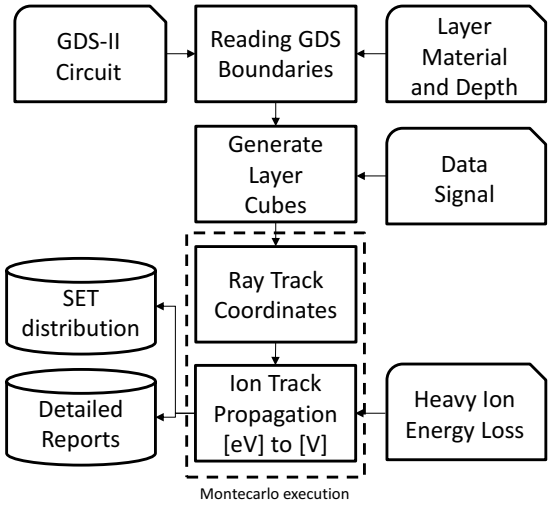

Fig. 3. The Rad-Ray execution flow from the GDS-II circuit cell description to the SET distribution and detailed reports.

The first phase of the tool consists in generating the 3D structure derived from the GDS-II circuit layout description of the cell. During this phase, the Rad-Ray tool translates the GDS description into a 3D mesh where boundaries are aligned in space and assigned to the respective layer material and depth. This phase is executed by the reading GDS boundaries function that generates the 3D geometrical structure under analysis and the size and shape of metallization and volumes of the cell. The second phase consists of generating the lattice mesh for every volume of the cell. This phase is executed by the Generate Layer Cubes function that creates a lattice of nodes depending on the type of material used for each volume space of the cell. In detail, each node is described with a charge value and an eV coefficient that will be computed during the heavy ion track analysis. The total number of nodes per volume matches the type of material. For instance, an inter-poly Silicon (SiO_2) has a lower density of nodes with respect to a Si_3N_4 junction. The third phase consists of the Monte Carlo analysis that is described in the following subsection.

The Rad-Ray tool uses a set of ancillary files to perform the creation of the 3D mesh and for the execution of the Monte Carlo analysis. The ancillary information includes the layer

material structure and depth related to the technology used by the cell under investigation, the data signal used to annotate the bias condition of the cell and finally, the heavy ion energy loss for each Ion with respect to the material. An example of a result from this phase is illustrated in Fig. 4 where it is possible to observe the 3D geometrical structure under analysis and the size and shape of metallization and volumes of the cell.

A. Heavy Ion Track Analysis

Once the node lattice model of each volume is created, a Monte Carlo analysis of the heavy ion tracks passing through the cell space is performed. The first step consists in generating a list of starting and ending coordinates for each particle. It is possible to generate perpendicular particles, in order to mimic the ion ray generally provided by an accelerator, or at any kind of angle of the volume to simulate the heavy ion effects in space. After the generation of coordinates, the tool iteratively executes each ion particle track passage into the volumes. The resolution of the propagation-step is ~1 Å. During each propagation step, the heavy ion particle is simulated as a node in a given coordinate with a specific value of energy that is progressively released into each volume lattice node. The relative amount of energy loss for each volume is computed using the information contained in the third ancillary file that provides the eV/Å energy loss value per each type of material compound. The propagation terminates once the simulated particle reaches the final coordinate.

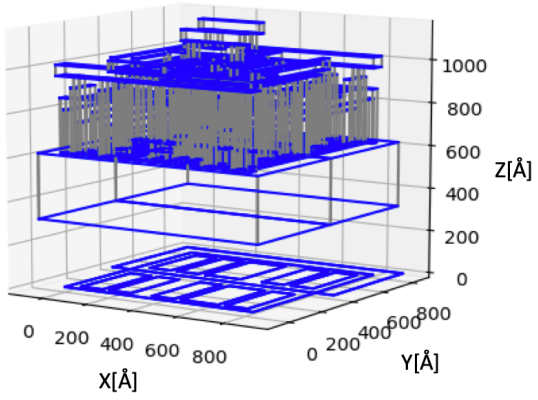

Fig. 4. An example of 3D volumetric structure generated by the proposed approach. Please note that each volume includes the relative lattice mesh structure. The unit of all axes is Å.

B. Released Charge Analysis

At the end of the particle propagation, each volume lattice node has the amount of charge released during the particle track. An example of this phase is illustrated in Fig. 5, where it is possible to observe the trajectory of the simulated heavy ion particle and the correspondent charged nodes affected during its propagation through the material. Please note that the colors are expressed in the form of a heat map: white color indicates the minimal amount of charge, red color indicates the maximal amount of charge.

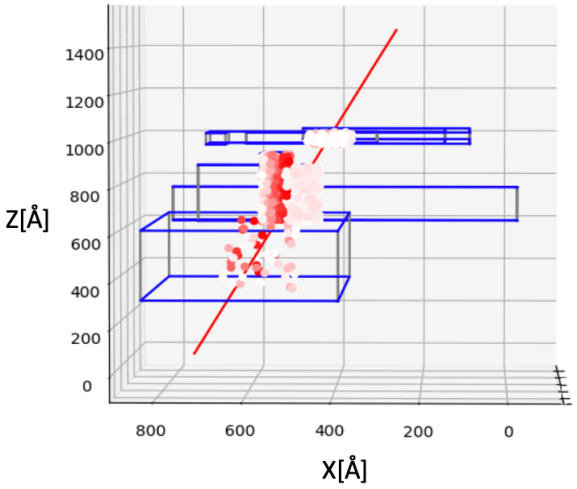

Fig. 5. A Heavy-Ion track releasing charge during its propagation. Colored spots provide the value of the correspondent released charge distributed for each cell volume.

C. Charge Propagation Algorithm

The distributed charge is propagated using a discretization algorithm that computes the charge value of each node to the neighborhood-discharged nodes in all six directions with a time resolution of 1 ps. During each step of the discretization, charges are progressively released into the overall node lattice.

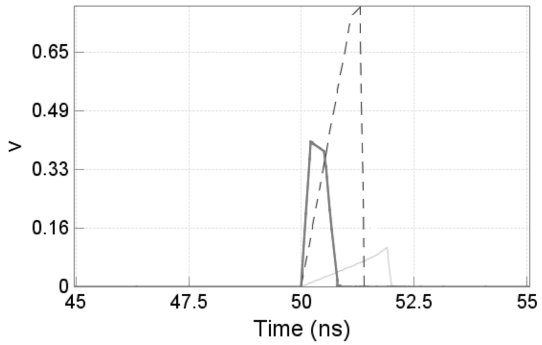

(a)

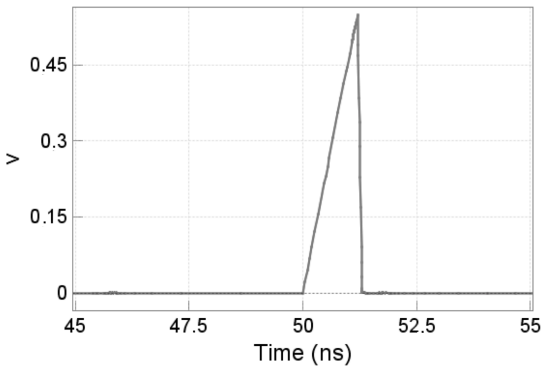

(b)

Figs. 6. The outcome of the Rad-Ray tool (visualized via H-Spice simulation) related to a single particle strike within the cell under analysis affecting three layers and reporting the related voltage level (a) and the cell output voltage level (b).

The charge propagation is calculated on the basis of the node lattice material and on the type of bias condition applied to the cell. The first aspect is tuning the amount of charge released into the specific node volume while the second aspect is applied to the direct calculation of the Voltage drift on the output of the cell. This avoids the representation of a transient pulse that overlaps with the original voltage state of the cell. The bias model actually used is static.

This method permits the computation of the voltage levels generated by the heavy ion track traversing each volume of the analyzed circuit. Finally, the method converts the charge into Volts and plots the output voltage value of the volumes related to the cell output signals. The result is an effective plot of the transient pulse at the output of the analyzed cell. As an example, in Fig. 6a, three different voltage values related to the inverter cell metal layers are illustrated using H-Spice tool; while Fig. 6b illustrates an example of transient pulse generated at the output of the corresponding cell. The voltage values generated by the Rad-Ray tool include the effect of the metallization inherent to the cell under analysis.

V. Experimental Analysis and Results

The analysis we performed consisted of two different experiments. The first one has been a radiation test campaign performed at the Université Catholique de Louvain (UCL) Heavy Ions Facility on a test circuit consisting of four test chains mapped on a SmartFusion2 (SF2) Flash-based FPGA. The goal has been to measure the sensitivity to transient errors and more in particular to SETs of each specifically designed chain. The second analysis consisted in the layout modeling of the inverter chain implemented by Look-Up Table (LUT) resources, D-type Flip-Flop (DFF) on the SF2 device and to perform a comparative analysis with respect to the results obtained using the Rad-Ray tool, in particular, in relation to the Single Event Transient (SET) cross-section per LUT.

A. Heavy Ion Radiation Test Experiments

We performed a radiation test campaign at the Cyclotron of the UCL on a SmartFusion2 (SF2) FPGA (M2S150TS-FC1152) mounted on the SF2 advanced development kit. The test circuit contains 4 chains, each one consisting of 2,000 Flip-Flops all clocked at 50MHz where each pair of FFs is separated by 4, 8 and 16 inverter gates in a row. A control and monitor system has been implemented using a Xilinx Zynq-based board to automatize the experiment and monitor the chain outputs of the DUT by counting the number of transient events. A picture of the setup adopted is shown in Fig. 7.

The test equipment consists of a monitor board based on a Xilinx Pynq-Z2 board which monitors the DUT devices and communicates with the external host computer. The chain input signals are controlled (grounded during test) by the monitor board which also observes and stores the outputs of the chains, the current and the temperature of the device during test. Different power supplies were used for the SF2 board and the Xilinx Pynq-Z2 board to manage the power cycle during the test execution. Oscilloscopes were used to monitor and store the voltage and current values of the SF2 board (via different test points) and to detect any anomalies happening during the radiation test. A separate power supply was used to provide thermal resistor power to maintain the DUT at the specified test temperature. During the execution of each test run, data related to the current absorbed by the DUT are monitored and stored by the monitoring board with a sampling rate of around 2 kHz and by an external scope.

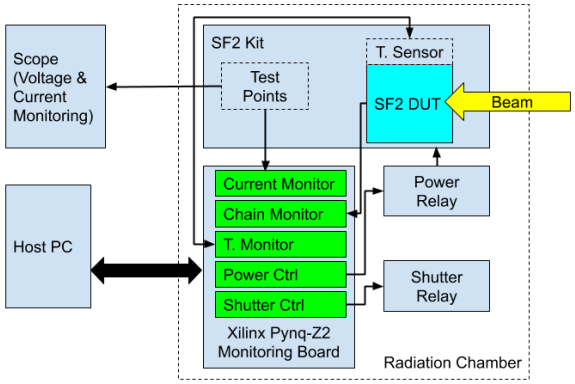

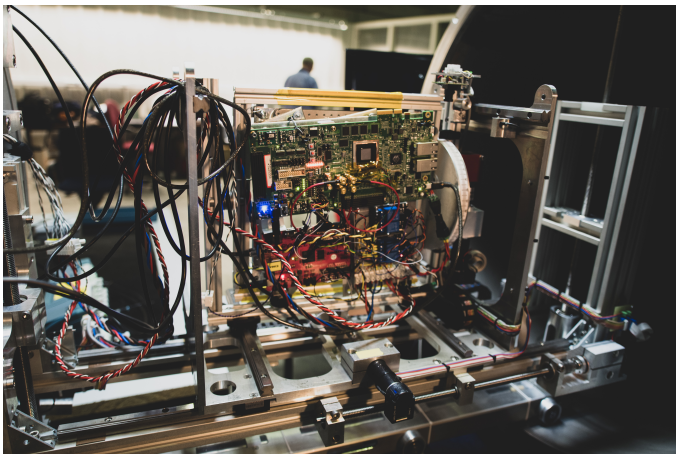

Figs. 7. A scheme and a picture of the radiation-test setup installed at the UCL beam-chamber consisting of the SF2 under test and the Pynq-Z2 monitoring board.

TABLE I
CHARACTERISTICS OF THE USED BEAM

Ion	DUT Energy [MeV]	Range [µm Si]	LET At surface [MeV/mg/cm²]	LET at sensitive volume [MeV/mg/cm²] Sample Thickness	
				61µm	67µm
$^{22}Ne^{7+}$	238	202.0	3.3	3.3	3.3
$^{27}Al^{8+}$	250	131.2	5.7	7.2	7.4
$^{40}Ar^{12+}$	379	120.5	10.0	13.6	14.2
$^{58}Ni^{18+}$	582	100.5	20.4	27.5	28.6
$^{84}Kr^{25+}$	769	94.2	32.4	40.1	40.6

The host PC has been used to store and control the execution of the test. In particular, the main operations executed by the host PC have been: real-time monitoring of

the channel outputs, current values and temperature through a GUI application; control of the experiment through a Python interface in order to follow the voltage and temperature values and to allow the identification of anomalies. We performed the radiation test using the beam reported in Table I, and the characteristics of the chains used are described in Table II. The beam flux has been fixed to 10^4 particles/s•cm^2. The homogeneity is ± 10 % on a 25 mm diameter.

TABLE II
CHARACTERISTICS OF THE CHAINS

Circuit Channel [#]	Design Details	FFs [#]	INVs [#]
Ch. 0	FFs	2,000	0
Ch. 1	FFs+4 INVs	2,000	8,000
Ch. 2	FFs+8 INVs	2,000	16,000
Ch. 3	FFs+16 INVs	2,000	32,000

During the experiment, we collected the following SET events: 1,274 for channel 0; 4,514 for channel 1; 8,568 for channel 2 and 16,947 for channel 3. The large sample size results in a low variation in experimental results. However, we observed small error differences attributed to the variability of the routing topology between the logic chains. The results of the cross-section for each chain are illustrated in Fig. 8, please note that LET values are related to the computed LET at the device surface, as calculated in Table I. Figs. 9 and 10 show cross-section of the FF and each INV gate. The results permit the identification of the individual contributions of the inverters and the FF.

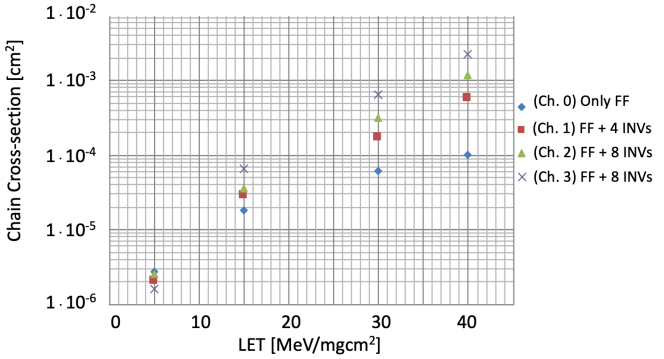

Fig. 8. The cross-section per circuit channel computed on the overall number of observed Single Event Transient (SET) effects.

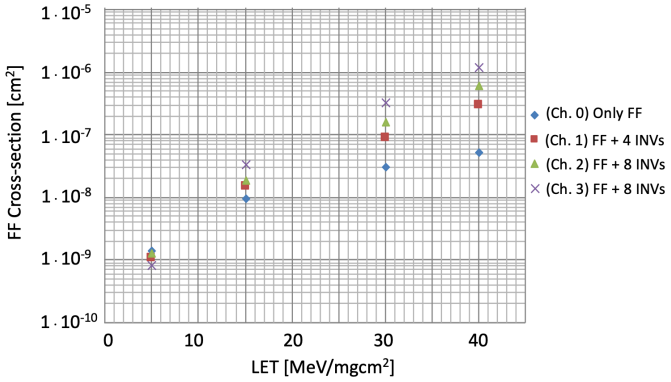

Fig. 9. The computed Flip-Flop cross-section per circuit channel on the overall number of observed Single Event Transient (SET) effects.

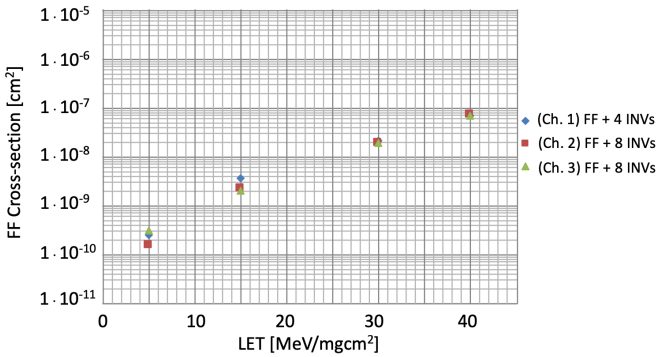

Fig. 10. The computed Inverter cross-section per circuit channel on the overall number of observed Single Event Transient (SET) effects.

The test results show that the inverters introduce an increase of the design chain cross section up to one order of magnitude at the LET of 40 MeV/mg/cm^2 corresponding to the Kr ion. This effect is progressively reduced for lower LETs, since the generated SETs are progressively shorter and with a lower amplitude, the contribution of the Propagation Induced Pulse Broadening (PIPB) is attenuated.

We measured the INV cross-section comparing exclusively the channels including inverters by normalizing the PIPB effect. We considered that the impact of PIPB has a threshold around 10 MeV/mg/cm^2, below this value the contribution of the PIPB become negligible. Considering the PIPB normalization the inverter cross-section shown in Fig. 10 provides an equivalent cross-section between all the different chains in the design.

B. 3D-Simulation Analysis and Comparison

Once the node lattice model of each volume is created, a Monte Carlo analysis of the heavy ion tracks passing through the cell space is performed.

We develop a 65 nm LUT layout design of a four-input LUT that has been designed according to the Microsemi model and using the Nan-Gate Open Cell library [18] at 65 nm. The 4-input LUT can be configured to implement any 4-input combinational function where the output is XORed with a carry chain and with an output sum. For the purpose of this work, we did not use the carry lines. Prior to performing the analysis, the LUT functionality was verified for behavior and timing, using the Microsemi tool and HSPICE post layout simulations.

We performed two types of analysis. The first consisted in emulating the heavy ion radiation cocktail used during the radiation campaign. For this purpose, we settled on a simulation of 10,000 particles per each type of heavy ion, and analyzed independently the Flip-Flop and the LUT layout models. Our method provided an analysis with a deviation error to the measurement lower than $2 \cdot 10^{-9}$. The results obtained when analyzing the Flip-Flop are reported in Fig. 11. Based on a comparison of the test and simulation results it can be stated that the proposed method can provide accurate cross-section predictions and missing cross-section versus LET points. We observed a pessimistic calculation of the cross-section for higher LET values. In particular, as illustrated in Fig. 12, at higher LET (>30 MeV/mgcm^2) differences between

the test data and simulations results were noted and attributed to process variations in the design that are not currently captured by the model.

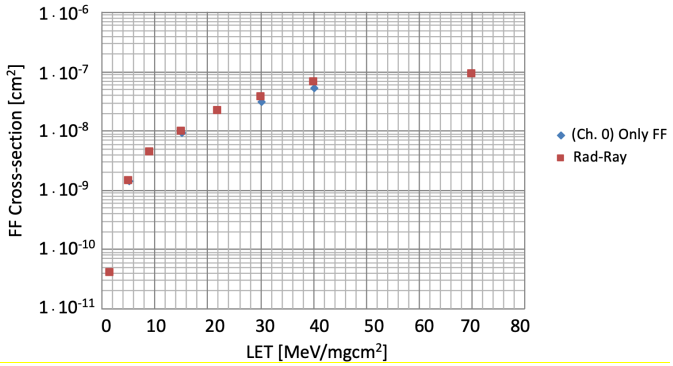

Fig. 11. The cross-section calculation per Flip-Flop of the SmartFusion2 65 nm technology analysis of our method and the results obtained from the radiation test on the Design Channel 0 (Only Flip-Flops).

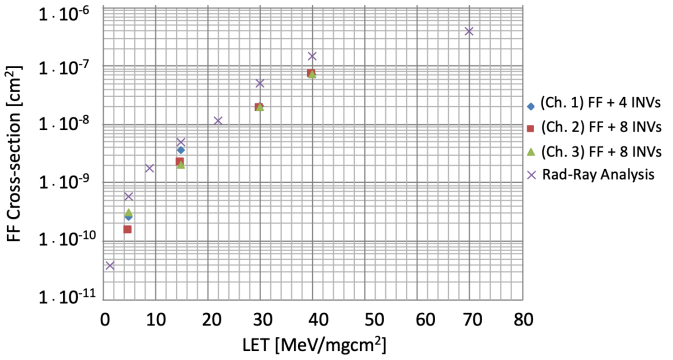

Fig. 12. The cross-section per LUT (implementing the Inverter function) of the SmartFusion2 65 nm technology obtained by the radiation test and by the Rad-Ray analysis.

The computational time requested by our simulation to analyze the complete heavy ion spectrum has been 8.6 hours of execution time on a PC with a generic 64-bit dual-core processor and 8GB of RAM. The LUT analysis was performed using 5,000 particles per heavy ion type due to increased time to perform each computation. The LUT model consist of 2,936 different volumes distributed among 23 layers, the materials used for each layer were inferred partially based on the Flash-cell information [19]. Finally, an exhaustive investigation of all sensitive volumes of the two most dominant cells, FF and MUX2, was accomplished in an effort to ascertain the differences between the test data and analytical results shown in Fig. 12. In this case, the computational time requested by the simulation to analyze the complete heavy ion spectrum has increased to 34.3 hours.

As shown in Fig. 12, our method provides a slightly pessimistic computation of the SET cross-section with respect to the cross-section obtained from radiation tests. We think that this is due to the possible differences of the routing model developed for the LUT. In order to have a better investigation of this phenomenon, we performed a second analysis with our method. We performed an exhaustive scan of all the sensitive volumes of two more relevant cells under analysis: the FF and the MUX2. Please consider that the MUX2 is the main cell composing the overall LUT-4 model adopted for the radiation test comparative analysis. For the purpose of this analysis, we used the most energetic ion, and the tool has been configured in order to provide a heat-map of the analyzed cell with the goal of identifying the most sensitive volumes and to observe the ranges of SETs generated by the analysis.

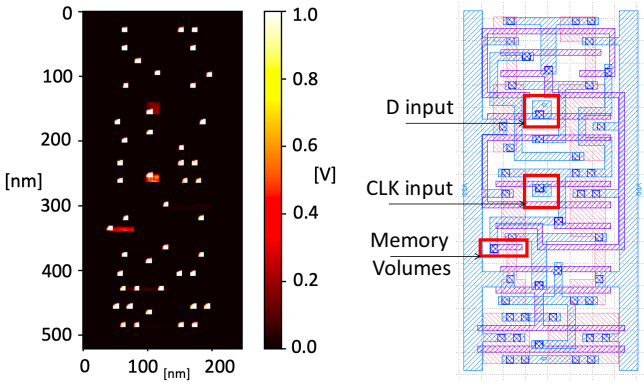

Figs. 13. The Single Event Transient (SET) sensitivity heat-map from the top view of the 65 nm Flip-Flop cell under investigation (a). The correspondent top-level layout view of the FF cell under analysis (b).

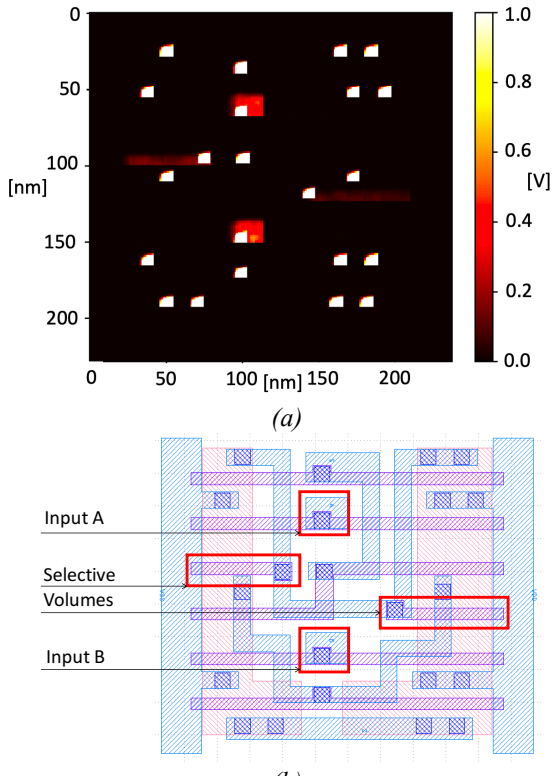

Figs. 14. The Single Event Transient (SET) sensitivity heat-map from the top view of the 65 nm MUX2 cell under investigation (a). The correspondent top-level layout view of the MUX2 cell under investigation (b).

The analyses were performed by simulation of the Xe heavy ion track for each nm^2 of the cell volumes. The results of the exhaustive heavy ion scan of the two cells are illustrated in Figs. 13 and 14.

Figs. 13a and 14a provide an accurate heat-map of the sensitive volumes of the cell, where the voltage values are normalized to be between 0 and 1 Volt. Furthermore, Fig. 13.b

and Fig. 14.b provide the top view of the functional layers, particularly metal layers 9 and 11 and junction volumes 10. Interestingly, the junction volumes are extremely sensitive to the heavy ion particle. As shown by the heat-map, when a heavy ion crosses a junction volume the released charge provokes voltage glitches of the maximal amplitude.

When the FF cell analysis is considered, three other portions of the cell volumes are critical: D input signal, CLK input signal and memory storage volumes. The overall sensitive volume corresponds to about 8% of the total area.

Similarly, we performed the analysis on the main cell of the 4-input LUT design: the MUX2. Also, in this case, we observed that junction volumes are extremely sensitive to heavy ions. Besides, the sensitive regions are dominated by three functional areas: input signal A and input signal B and the volume related the memory storage values. The overall sensitive volume corresponds to about 13% of the total area.

VI. Conclusions

This paper describes a TCAD tool that has been developed to provide 3-D analysis of the heavy ion SET response of advanced digital circuits. The main innovation of the developed approach is the capability to simulate the heavy ion tracks considering the different material volumes of a cell and to execute the charge sharing distribution and propagation among the different volumes. The proposed approach can be applied also to Physical Design Kit (PDK) libraries for ASIC implementation ranging from 45 nm to 130 nm. In the present work, we performed a first evaluation of the developed approach tool thanks to an accurate model of a 4-input LUT and a Flip-Flop sequential element implemented using a Flash-based technology of 65 nm. We compared the analysis with heavy ion radiation test campaigns performed at UCL. The results confirmed the accuracy of the method. Thanks to the proof-of-concept of the presented approach, the methodology can be adopted to extended types of effects that can be analyzed by 3D simulation methods such as Total Ionizing Dose (TID) and Single Event Latch-Up (SEL). Furthermore, the presented methodology is fundamental for the realization of ad-hoc radiation hardening solutions applied at the layout and circuit level.

VII. Acknowledgements

We thank M. Colucci, S. Francola and R. Mancini from Thales Alenia Space, Italy for their support for the realization and execution of the radiation test experiments.

References

[1] J. R. Ahlbin, L. W. Massengill, B. L. Bhuva, B. Narasimham, M. J. Gadlage and P. H. Eaton, "Single-Event Transient Pulse Quenching in Advanced CMOS Logic Circuits," *IEEE Trans. Nucl. Sci.*, vol. 56, no. 6, pp. 3050-3056, Dec. 2009.

[2] J. R. Ahlbin et al., "The Effect of Layout Topology on Single-Event Transient Pulse Quenching in a 65 nm Bulk CMOS Process," *IEEE Trans. Nucl. Sci.*, vol. 57, no. 6, pp. 3380-3385, Dec. 2010.

[3] J. R. Ahlbin et al., "Double-pulse-single-event transients in combinational logic," 2011 *International Reliability Physics Symposium*, Monterey, CA, 2011, pp. 3C.5.1-3C.5.6.

[4] O. A. Amusan et al., "Charge Collection and Charge Sharing in a 130 nm CMOS Technology," *IEEE Trans. Nucl. Sci.*, vol. 53, no. 6, pp. 3253-3258, Dec. 2006.

[5] V. Ferlet-Cavrois et al., "Statistical Analysis of the Charge Collected in SOI and Bulk Devices Under Heavy Ion and Proton Irradiation—Implications for Digital SETs," *IEEE Trans. Nucl. Sci.*, vol. 53, no. 6, pp. 3242-3252, Dec. 2006.

[6] S. DasGupta, A. F. Witulski, B. L. Bhuva, M. L. Alles, R. A. Reed, O. A. Amusan, J. R. Ahlbin, R. D. Schrimpf and L. W. Massengill, "Effect of Well and Substrate Potential Modulation on Single Event Pulse Shape in Deep Submicron CMOS," *IEEE Trans. Nucl. Sci.*, vol. 54, no. 6, pp. 2407– 2412, Dec. 2007.

[7] V. Ferlet-Cavrois, P. Paillet, D. McMorrow, N. Fel, J. Baggio, S. Girard, O. Duhamel, J. S. Melinger, M. Gaillardin, J. R. Schwank, P. E. Dodd, M. R. Shaneyfelt, and J. A. Felix, "New insights into single event transient propagation in chains of inverters. Evidence for propagation-induced pulse broadening," *IEEE Trans. Nucl. Sci.*, vol. 54, no. 6, pp. 2338–2346, Dec. 2007.

[8] V. Ferlet-Cavrois, V. Pouget, D. McMorrow, J. R. Schwank, N. Fel, F. Essely, R. S. Flores, P. Paillet, M. Gaillardin, D. Kobayashi, J. S. Melinger, O. Duhamel, P. E. Dodd, and M. R. Shaneyfelt, "Investigation of the propagation induced pulse broadening (PIPB) effect on single event transients in SOI and bulk inverter chains," *IEEE Trans. Nucl. Sci.*, vol. 55, no. 6, pp. 2842–2853, Dec. 2008.

[9] L. Sterpone, N. Battezzati and V. Ferlet-Cavrois, "Analysis of SET Propagation in Flash-Based FPGAs by Means of Electrical Pulse Injection," *IEEE Trans. Nucl. Sci.*, vol. 57, no. 4, pp. 1820-1826, Aug. 2010.

[10] L. Sterpone, N. Battezzati, F. L. Kastensmidt and R. Chipana, "An Analytical Model of the Propagation Induced Pulse Broadening (PIPB) Effects on Single Event Transient in Flash-Based FPGAs," *IEEE Trans. Nucl. Sci.*, vol. 58, no. 5, pp. 2333-2340, Oct. 2011.

[11] O. A. Amusan, A. L. Sternberg, A. F. Witulski, B. L. Bhuva, J. D. Black, M. P. Baze, L. W. Massengill, "Single event upsets in a 130 nm hardened latch design due to charge sharing," Proc. of the 45th *Int. Reliability Physics Symp.*, Arizona, 2007, pp. 306–311.

[12] R. C. Harrington et al., "Effect of Transistor Variants on Single-Event Transients at the 14-/16-nm Bulk FinFET Technology Generation," *IEEE Trans. Nucl. Sci.*, vol. 65, no. 8, pp. 1807-1813, Aug. 2018.

[13] H. Jiang, H. Zhang, J. S. Kauppila, L. W. Massengill and B. L. Bhuva, "An Empirical Model for Predicting SE Cross Section for Combinational Logic Circuits in Advanced Technologies," *IEEE Trans. Nucl. Sci.*, vol. 65, no. 1, pp. 304-310, Jan. 2018.

[14] G. Hubert and L. Artola, "Single-Event Transient Modeling in a 65-nm Bulk CMOS Technology Based on Multi-Physical Approach and Electrical Simulations," *IEEE Trans. Nucl. Sci.*, vol. 60, no. 6, pp. 4421-4429, Dec. 2013.

[15] M. Raine et al., "Impact of the Radial Ionization Profile on SEE Prediction for SOI Transistors and SRAMs Beyond the 32-nm Technological Node," *IEEE Trans. Nucl. Sci.*, vol. 58, no. 3, pp. 840-847, June 2011.

[16] S. Azimi et al, "SETA: A CAD Tool for Single Event Transient Analysis and Mitigation on Flash-Based FPGAs," 2018 15th *International Conference on Synthesis, Modeling, Analysis and Simulation Methods and Applications to Circuit Design* (SMACD), Prague, 2018, pp. 1-52.

[17] C. W. Gwyn, D. L. Scharfetter, and J. L. Wirth, "The analysis of radiation effects in semiconductor junction devices," *IEEE Trans. Nucl. Sci.*, vol. 14, no. 6, pp. 153–169, Dec. 1967.

[18] D. Binder, E. C. Smith, and A. B. Holman, "Satellite anomalies

from galactic cosmic rays," *IEEE Trans. Nucl. Sci*., vol. 22, no. 6, pp. 2675–2680, Dec. 1975.

[19] P. E. Dodd, "Physics-based simulation of single-event effects," *IEEE Trans. on Device and Materials Reliability*, vol. 5, no. 3, pp. 343-357, Sept. 2005.

[20] R. A. Reed et al., "Physical Processes and Applications of the Monte Carlo Radiative Energy Deposition (MRED) Code," IEEE *Trans. Nucl. Sci.*, vol. 62, no. 4, pp. 1441-1461, Aug. 2015.

[21] K. M. Warren et al., "The contribution of nuclear reactions to heavy ion single event upset cross-section measurements in a high-density SEU hardened SRAM," *IEEE Trans. Nucl. Sci.*, vol. 52, no. 6, pp. 2125-2131, Dec. 2005.

[22] K. M. Warren et al., "Integrating Circuit Level Simulation and Monte-Carlo Radiation Transport Code for Single Event Upset Analysis in SEU Hardened Circuitry," *IEEE Trans. Nucl. Sci.*, vol. 55, no. 6, pp. 2886-2894, Dec. 2008.

[23] K. M. Warren et al., "Heavy Ion Testing and Single Event Upset Rate Prediction Considerations for a DICE Flip-Flop," *IEEE Trans. Nucl. Sci.*, vol. 56, no. 6, pp. 3130-3137, Dec. 2009.

[24] L. Ding et al., "Modeling the Dependence of Single-Event Transients on Strike Location for Circuit-Level Simulation," *IEEE Trans. Nucl. Sci.*, vol. 66, no. 6, pp. 866-874, June 2019.